Title

Cone Structure Imaged With Adaptive Optics Scanning Laser Ophthalmoscopy in Eyes With Nonneovascular Age-Related Macular DegenerationAOSLO in Eyes With Nonneovacular AMD

Journal

Investigative Ophthalmology & Visual Science, 54(12)

ISSN

0146-0404

Authors

Zayit-Soudry, Shiri
Duncan, Jacque L
Syed, Reema
et al.

Publication Date

2013-11-15

DOI

10.1167/iovs.13-12433

Peer reviewed

Cone Structure Imaged With Adaptive Optics Scanning Laser Ophthalmoscopy in Eyes With Nonneovascular Age-Related Macular Degeneration

Shiri Zayit-Soudry,[1] Jacque L. Duncan,[1] Reema Syed,[1] Moreno Menghini,[1] and Austin J. Roorda[2]

[1]Department of Ophthalmology, University of California at San Francisco, San Francisco, California
[2]School of Optometry, University of California at Berkeley, Berkeley, California

Correspondence: Jacque L. Duncan, Department of Ophthalmology, University of California, San Francisco, 10 Koret Way, San Francisco, CA 94143-0730; duncanj@vision.ucsf.edu.

Submitted: May 18, 2013
Accepted: October 9, 2013

Citation: Zayit-Soudry S, Duncan JL, Syed R, Menghini M, Roorda AJ. Cone structure imaged with adaptive optics scanning laser ophthalmoscopy in eyes with nonneovascular age-related macular degeneration. *Invest Ophthalmol Vis Sci.* 2013;54:7498–7509. DOI:10.1167/iovs.13-12433

Purpose. To evaluate cone spacing using adaptive optics scanning laser ophthalmoscopy (AOSLO) in eyes with nonneovascular AMD, and to correlate progression of AOSLO-derived cone measures with standard measures of macular structure.

Methods. Adaptive optics scanning laser ophthalmoscopy images were obtained over 12 to 21 months from seven patients with AMD including four eyes with geographic atrophy (GA) and four eyes with drusen. Adaptive optics scanning laser ophthalmoscopy images were overlaid with color, infrared, and autofluorescence fundus photographs and spectral domain optical coherence tomography (SD-OCT) images to allow direct correlation of cone parameters with macular structure. Cone spacing was measured for each visit in selected regions including areas over drusen ($n = 29$), at GA margins ($n = 14$), and regions without drusen or GA ($n = 13$) and compared with normal, age-similar values.

Results. Adaptive optics scanning laser ophthalmoscopy imaging revealed continuous cone mosaics up to the GA edge and overlying drusen, although reduced cone reflectivity often resulted in hyporeflective AOSLO signals at these locations. Baseline cone spacing measures were normal in 13/13 unaffected regions, 26/28 drusen regions, and 12/14 GA margin regions. Although standard clinical measures showed progression of GA in all study eyes, cone spacing remained within normal ranges in most drusen regions and all GA margin regions.

Conclusions. Adaptive optics scanning laser ophthalmoscopy provides adequate resolution for quantitative measurement of cone spacing at the margin of GA and over drusen in eyes with AMD. Although cone spacing was often normal at baseline and remained normal over time, these regions showed focal areas of decreased cone reflectivity. These findings may provide insight into the pathophysiology of AMD progression. (ClinicalTrials.gov number, NCT00254605.)

Keywords: age-related macular degeneration, adaptive optics, cones, scanning laser ophthalmoscopy

Age related macular degeneration is the leading cause of vision loss in patients aged 65 years or older in developed countries.[1–3] Drusen, deposits of extracellular material accumulating between the RPE and the inner collagenous layer of Bruch's membrane, are among the earliest manifestations of AMD and can lead to progressive vision loss even in the absence of advanced disease.[4] Dynamic accumulation and regression of drusen is a risk factor for formation of geographic atrophy (GA) of the RPE, an atrophic form accounting for 35% of all late AMD cases.[5] Typically, one or more patches of atrophy of the outer retina, RPE, and choriocapillaris show enlargement and coalesce over time, accounting for moderate to severe vision loss.[6]

Although vision loss in AMD results from photoreceptor degeneration, the primary pathophysiologic mechanism leading to photoreceptor loss from progression of drusen and GA is still uncertain. Several lines of evidence suggest that RPE cell death is the key event in formation of GA, triggering subsequent atrophy of the choriocapillaris and loss of the overlying photoreceptors.[7–9] One of the factors suggested to initiate the disease process is accumulation of lipofuscin within RPE cells. Clinicopathologic studies have documented that continuous lipofuscin deposition in RPE cells at the margin of GA leads to cellular hypertrophy with resultant effects on cell metabolism and subsequent cell death.[6,10–12] Studies using fundus autofluorescence (FAF) imaging showed that lipofuscin-filled RPE cells at the GA margin correspond to a band of increased autofluorescence, which has been shown to represent a marker for future RPE cell loss and disease progression.[13] In contrast, several histologic studies have suggested that the photoreceptors play a principal role in the evolution of GA.[14–16] Photoreceptor degeneration and loss were suggested to occur before disease in the RPE/Bruch's membrane complex progresses.[17,18] Similarly, examination of postmortem eyes with AMD revealed structural photoreceptor changes overlying drusen,[15,16] and thinning of the photoreceptor layer over drusen was observed in spectral domain optical coherence tomography (SD-OCT) images of eyes

Table. Clinical Characteristics of the Study Patients at Baseline

Subject	AOSLO ID	Sex	Age, y	Eye	AMD Classification*	Visual Acuity Snellen	Visual Acuity ETDRS, Letters	Foveal Sensitivity HVF 10-2, dB
P1	30003	F	67	Right	Late (Nonfoveal GA)	20/25	80	31
P1	30003	F	67	Left	Late (Nonfoveal GA)	20/40	69	31
P2	30021	M	73	Left	Late (Nonfoveal GA)	20/20	83	33
P3	30024	F	68	Left	Late (Nonfoveal GA)	20/20	85	36
P4	30011	M	68	Left	Intermediate	20/16	90	36
P5	30023	M	50	Left	Intermediate	20/16 +3	93	37
P6	10052	M	71	Right	Intermediate	20/32 +3	78	29
P7	30005	M	64	Right	Intermediate	20/12.5	95	36

* AMD classification is based on the Clinical Classification System for AMD proposed by the Macular Research Classification Committee.[48]

with AMD,[19] suggesting correlation between drusen and focal photoreceptor cell death.

Examination of the retina over drusen and at the margin of GA may provide further insight into the structural changes preceding progression of AMD. The morphologic changes at GA margins associated with GA enlargement have been studied using a variety of retinal imaging modalities, including fundus photography,[20,21] FAF,[22,23] and OCT.[24–27] Adaptive optics

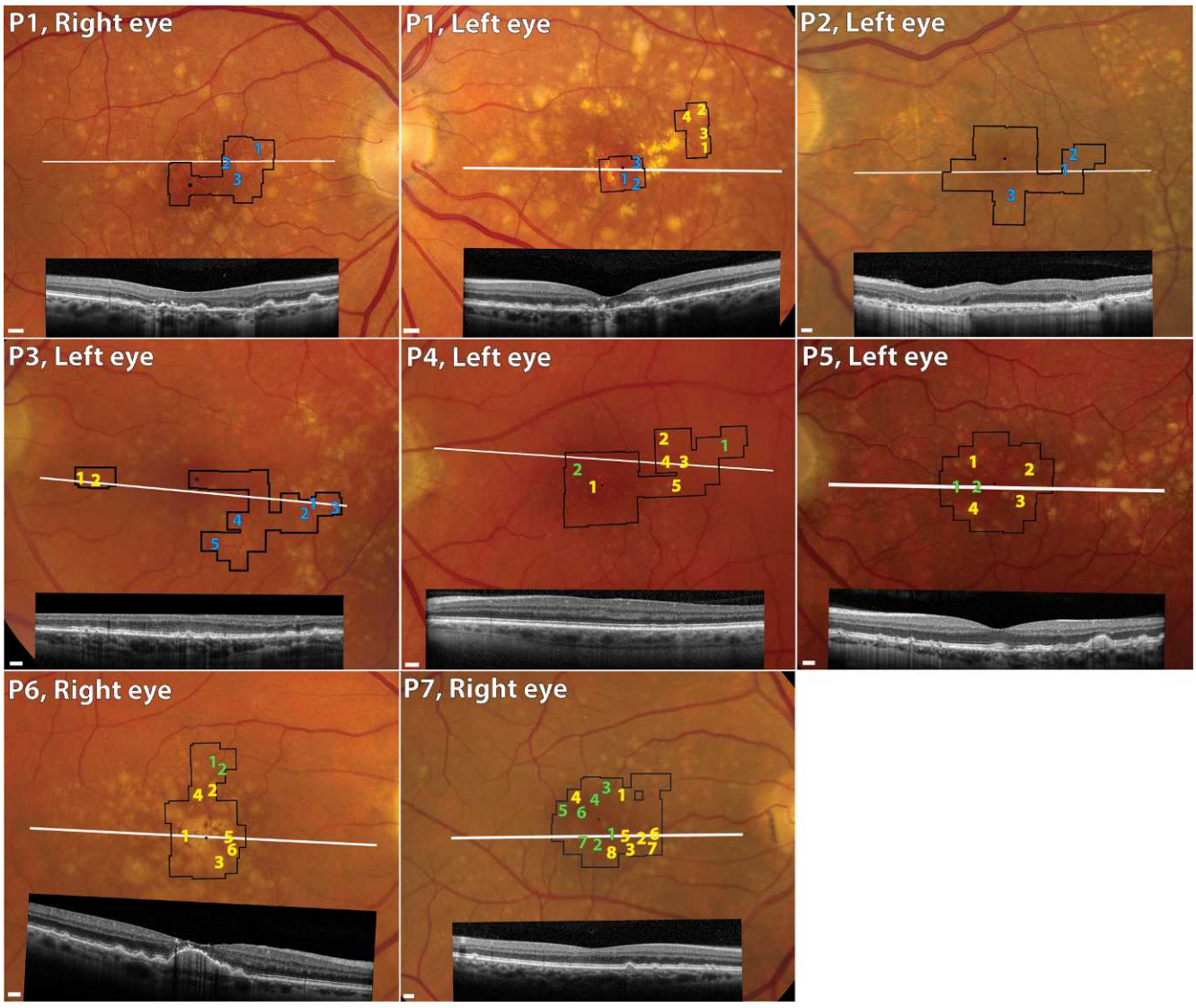

Figure 1. Clinical images and AOSLO outline. For each study patient, color fundus photograph obtained at baseline is shown with SD-OCT scan superimposed, and area imaged with AOSLO at baseline outlined in *black*. *White horizontal lines* represent location of OCT scan. *Black dot* denotes fixation. *Green, yellow,* and *blue numbers* within AOSLO image outline represent locations of ROIs where cone spacing was analyzed in each AOSLO image during the study (*Green*: intact retinal areas with no drusen or geographic atrophy, *yellow*: ROIs over drusen, *blue*: ROIs at the margin of geographic atrophy). *White scale bar* at lower left corner of each color fundus image: 200 μm.

Investigative Ophthalmology & Visual Science

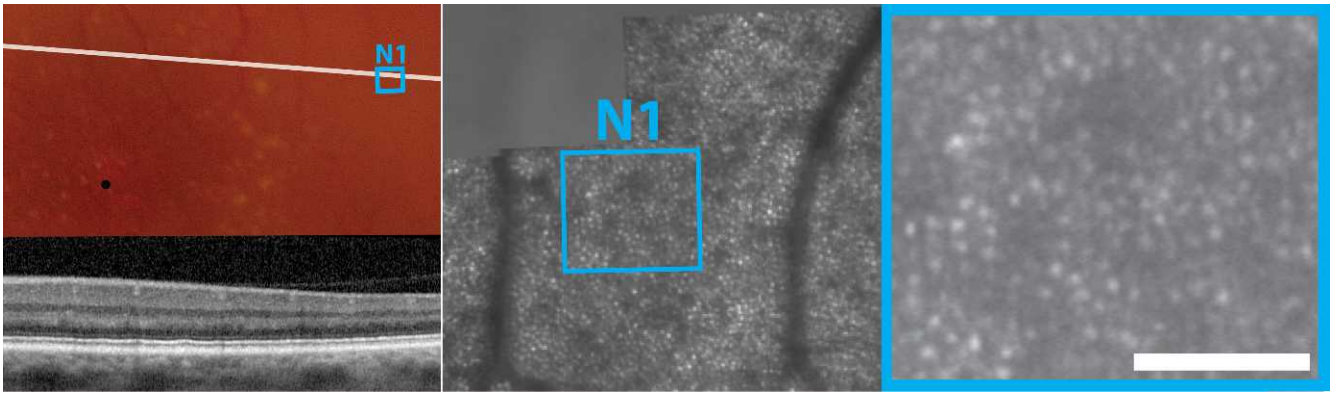

FIGURE 2. Morphologic features of AOSLO images from healthy retinal area in an eye with intermediate AMD. *Left*: color fundus photograph obtained at baseline from the left eye of patient 4 with registered SD-OCT scan. Optical coherence tomography line is indicated in *white*. Fixation is denoted by *black dot*. Area surrounding ROI N1 is outlined in *blue*. Color fundus image shows normal-appearing retinal area and OCT scan shows preserved outer nuclear layer (ONL), photoreceptor IS/OS and RPE layers. *Middle*: magnified AOSLO image registered on infrared fundus image, showing cones as bright profiles arranged into continuous mosaics. *Dark features* represent over-riding retinal vessels. *Right*: magnified AOSLO image of region N1. *Scale bar*: 15 arc minutes.

scanning laser ophthalmoscopy (AOSLO) is an imaging system that can noninvasively generate images of individual cone photoreceptors in living eyes.[28–31] The blur caused by the optical imperfections in living human eyes is the major factor limiting the ability to visualize photoreceptors with all methods commonly used in clinical practice. Adaptive optics can compensate for these ocular wavefront aberrations, and therefore increase the lateral resolution of retinal images to the order of 2 μm, allowing visualization of single cone photoreceptors. The feasibility of AOSLO imaging to generate in vivo images of macular cones has been shown in healthy eyes and eyes with inherited retinal degenerations.[32–36] Moreover, direct in vivo visualization of RPE cell mosaics was reported in eyes with inherited retinal degenerations in regions where cones were missing,[37,38] as well as in primate and human eyes using AOSLO autofluorescence images.[39] Thus, AOSLO imaging of eyes with AMD may allow detailed evaluation of the photoreceptor-RPE complex morphology and quantitative measures of macular cone structure adjacent to areas of incipient or existing GA. This information may enhance our understanding of the structural changes that occur in eyes with AMD and may provide a sensitive biomarker for disease progression in these eyes. Adaptive optics images from a single eye with nonneovascular AMD showed intact cone structure over drusen,[40] but in another study of four eyes with AMD AOSLO images revealed increasing levels of photoreceptor disruption that correlated with increasing disease severity.[41] The aim of the present study was to evaluate cone spacing over drusen and at GA margins in eyes with AMD using AOSLO in vivo imaging, and to correlate progression of AOSLO-derived cone spacing measures with standard measures of macular structure.

Materials and Methods

All research procedures were performed in accordance with the Declaration of Helsinki. The study protocol was approved by the institutional review boards of the University of California at San Francisco and University of California at Berkeley. All subjects gave written informed consent before participating in the study. Patients aged 50 years or older with intermediate AMD in at least one eye or late AMD manifesting nonfoveal GA and visual acuity of 20/40 or better were enrolled. If both eyes met the inclusion criteria, both eyes were studied. Patients were excluded if their pupils did not dilate to at least 7 mm, they had dense cataract or other media opacities, they had previously undergone ocular surgery, or they were unable to maintain stable fixation. Eyes with a history of neovascular AMD or retinal disease other than AMD at baseline were also excluded from the study.

All patients were imaged at baseline and thereafter returned for at least one follow-up visit with the last study visit occurring between 12 and 21 months after enrollment. At each study visit, each patient underwent complete eye examination including determination of best-corrected visual acuity as measured using standard methods used in the Early Treatment of Diabetic Retinopathy Study (ETDRS). Imaging studies included SD-OCT (Spectralis HRA-OCT; Heidelberg Engineering, Vista, CA), color fundus photography, and FAF. Fluorescein angiography was recorded at least once for each patient during the course of the study to document the presence of a window transmission defect consistent with GA and exclude the presence of choroidal neovascularization using a digital system (Topcon 50 EX fundus camera; Topcon Medical Systems, Oakland, NJ).

High quality clinical images generated with each imaging modality were selected from each patient visit, and registered with a baseline color fundus photograph selected for each eye using I2K Align software (Dual Align LLC, Clifton Park, NY). The registered overlays were used to guide selection of regions of interest (ROIs) for AOSLO imaging and analysis. Specifically, ROIs were selected in retinal locations without evidence of drusen or GA on fundus photography or SD-OCT, over drusen, and at GA margins. At baseline and at each study visit, the presence of photoreceptors in each selected ROI was verified by visualization of the inner segment-outer segment (IS/OS) junction or inner segment ellipsoid zone[42] in registered SD-OCT scans.

To determine correlation between progression of AOSLO-derived cone measures and standard measures of macular structure, drusen morphology, and height at each ROI were assessed at each visit.[43] Briefly, drusen height was derived from registered SD-OCT raster images that cut through the apex of the druse, and was measured manually using the ruler tool on Photoshop (Adobe Photoshop; Adobe Systems Inc., Mountain View, CA). Changes of 30% increase or decrease in drusen height during the study period were identified as progression or regression.[43] Similarly, registered horizontal SD-OCT scans

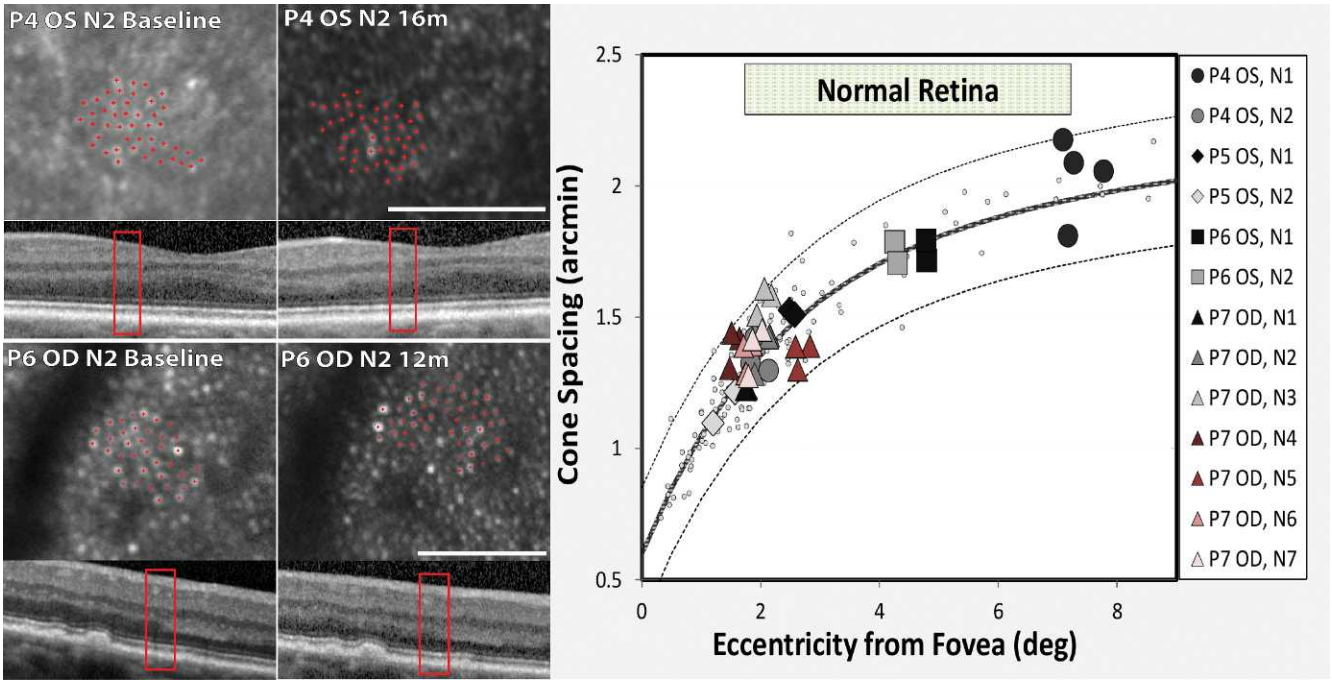

Figure 3. Cone spacing measurements in eyes with nonneovascular AMD at retinal regions showing no evidence of drusen or geographic atrophy. *Right*: cone spacing measures from nonneovascular AMD patients and healthy subjects versus retinal eccentricity. Each ROI was imaged at several follow-up visits, thus, multiple symbols are shown to represent the serial measures of cone spacing obtained from each ROI as listed in the legend on the *right*. Data from age-matched healthy subjects are plotted as *small gray dots. Dark solid line* indicates best fit to normal data. *Dashed lines*: 95% confidence limits of the best fit. *Left images*: AOSLO images and corresponding SD-OCT scans obtained from healthy retinal regions at baseline and at the last follow-up visit for that patient. Individual cones within mosaics identified in each AOSLO image are denoted by red cross-hairs. *White scale bar*: 15 arc minutes. *Red box* on OCT images denotes the area for which a corresponding magnified AOSLO image is shown above. *Upper panel*: patient 4, left eye, region N2. Cone spacing was measured at different locations of the cone mosaic identified within the same ROI between the visits where cones were unambiguously seen. Spectral domain optical coherence tomography images show normal outer retinal layers at the ROI. *Lower panel*: patient 6, right eye, location N2. Registered SD-OCT images show normal outer retinal morphology within the ROI that remained unchanged during the study period. *Large dark features* at the *left area* of each AOSLO image represents shadowing from a retinal blood vessel. Cone spacing values obtained from all normal regions were normal at baseline and remained within the normal range during the study.

through the drusen apex were inspected to qualitatively assess the integrity of the IS/OS layer, noting discontinuity and changes in reflectivity occurring focally or diffusely directly over the druse.[43]

AOSLO Image Acquisition and Processing

All patients underwent AOSLO imaging. Briefly, the AOSLO system makes use of a low-coherence, 840-nm light source, a Shack-Hartmann wavefront sensor, and a 140-actuator micro-electromechanical (MEMS) deformable mirror (Boston Micromachines Corporation, Watertown, MA). Digital videos were recorded in a continuous fashion throughout the central macular area, with special attention to regions of interest selected for each study eye. Each video subtended an area of 1.2° square.

Distortions in images caused by eye movements were minimized from each video with the use of customized software.[44,45] After correction, static frames were averaged to increase the signal-to-noise ratio. These images were then arranged (Adobe Photoshop; Adobe Systems, Inc.) by aligning landmarks on overlapping images to create a continuous montage of macular cones. Image scales were computed from calibration images recorded before each imaging session, to achieve a ratio of 420 × 420 pixels per degree in the final AOSLO montage. For each eye, AOSLO montages from each patient visit were superimposed upon all available clinical fundus images generated with each imaging modality at each visit (Adobe Illustrator; Adobe Systems, Inc.).

Cone Spacing Analysis

High-resolution AOSLO images were analyzed using customized software to determine cone spacing measures using previously described methods.[34,46,47] Briefly, each image was interpreted for the presence of features consistent with cone mosaics, including a polygonal array of uniformly-sized bright round or oval profiles. Each image was assessed by two investigators (SZS and AR) to minimize possible errors in cone identification (such as misidentification of cones or false identification of rods as cones). Cone spacing measures calculated for each selected region were compared with normative, age-similar values derived from nine visually healthy subjects aged 50 to 75 years (mean 60.7 ± 9 years) at similar retinal eccentricities. An exponential function was fit to the spacing of the normal data:

$$\text{Cone spacing} = A\exp(B{*}\text{eccentricity}) + C\exp(D{*}\text{eccentricity})$$

where A, B, C, and D are constants. Confidence intervals (CI; 95%) were estimated using the Matlab curve fitting toolbox (The MathWorks, Naticks, MA). The Z-score for each cone spacing measurement was computed as the number of SDs from the best fitting line to the normal data for that

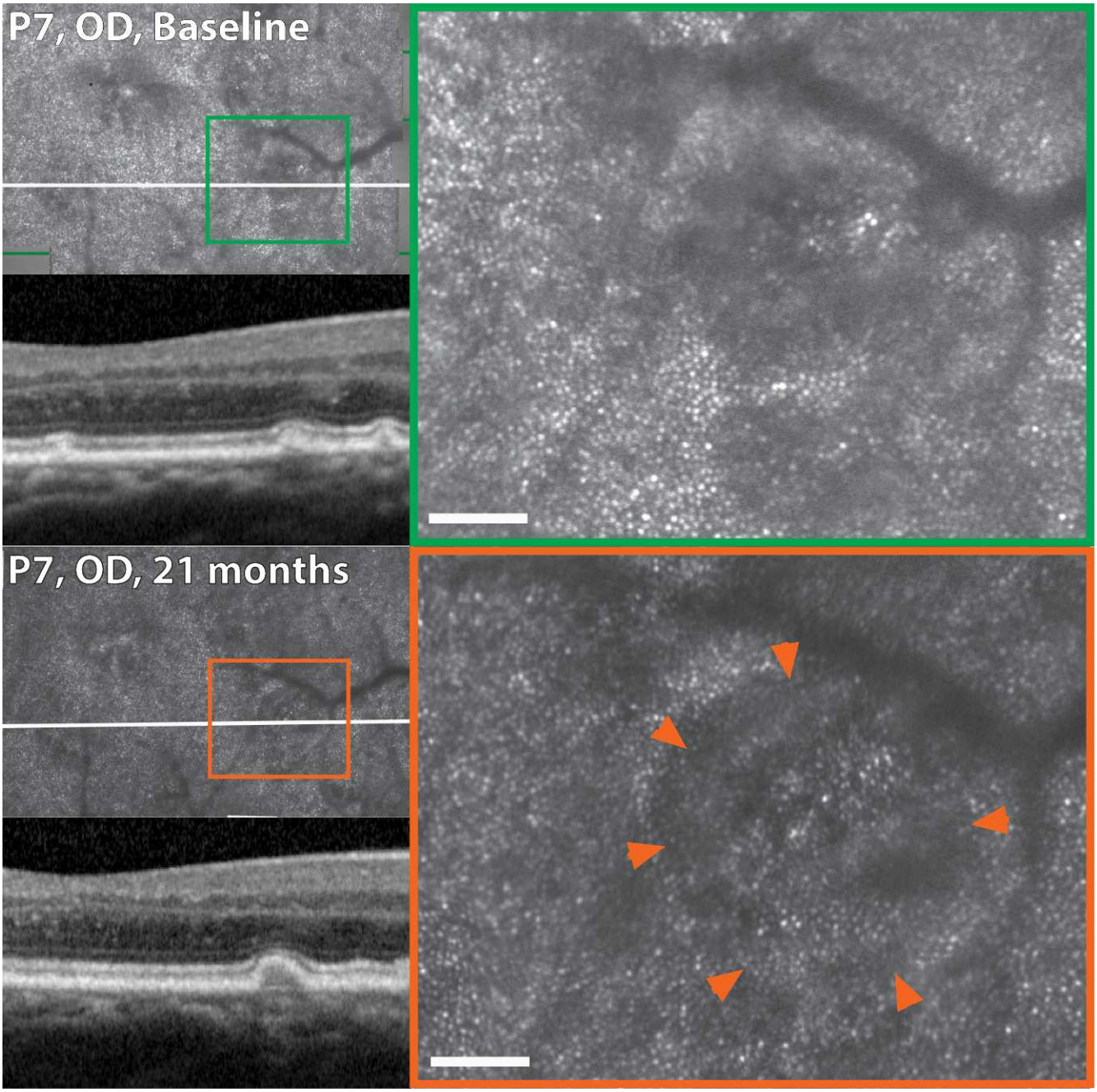

FIGURE 4. Morphologic features of AOSLO images from retinal areas over drusen in eyes with nonneovascular AMD. AOSLO images from region D12 of patient 7 obtained at baseline and after 21 months of follow up are registered with Heidelberg SD-OCT scans. The exact OCT scan location is indicated by the *white line*. The *green* and *orange boxes* indicate areas of the magnified AOSLO images shown in *green* and *orange insets*, respectively. *Scale bar*: 15 arc minutes.

eccentricity. Z scores higher or lower than a value of 2 were considered abnormal.

RESULTS

The study population consisted of eight eyes from seven patients with AMD, including four eyes with late AMD manifesting nonfoveal GA and four eyes with large drusen consistent with intermediate AMD at baseline (Table). The nomenclature used in our study is consistent with the clinical classification system for AMD.[48] Five of the seven patients were male, and ages at baseline ranged from 50 to 73 years (mean 65.8 ± 7.3 years). One patient had bilateral late AMD with nonfoveal GA in whom both eyes were included in the study. Visual acuity in the eight eyes at baseline ranged from 20/12.5 to 20/40 (ETDRS letters: 69–95). Figure 1 shows clinical retinal and SD-OCT images obtained at baseline for all study subjects, with the location of ROIs selected for AOSLO imaging denoted for each eye. Overall, ROIs identified and further analyzed in the entire study group included 13 sites exhibiting no GA or drusen on clinical examination or standard retinal imaging, 28 sites located over drusen, and 14 sites adjacent to GA margins.

Investigative Ophthalmology & Visual Science

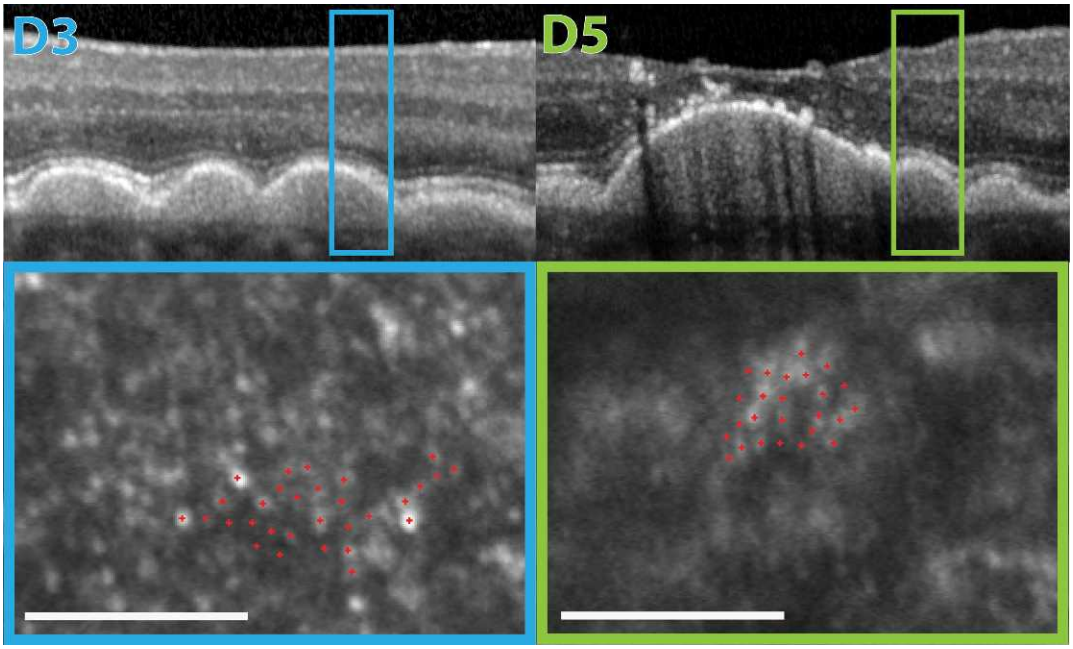

FIGURE 5. Adaptive optics scanning laser ophthalmoscopy images from regions over drusen at which cone spacing values were marginally increased at baseline compared with normal. Shown are two ROIs from the right eye of patient 6 (D3, D5). For each ROI, the corresponding SD-OCT and magnified AOSLO images are shown in the *upper* and *lower panels*, respectively (region D3: *Light blue*; region D5: *Light green*). *Box* on OCT cross-section image denotes the exact location of the ROI analyzed. *Scale bar* on AOSLO images: 15 arc minutes.

During the study period, three patients [P1 OS, P4 OS, P7 OD] manifested unstable fixation secondary to progression of macular degeneration or visually significant cataract, resulting in decreased AOSLO image quality obtained at some ROIs at some follow-up visits. Adaptive optics scanning laser ophthalmoscopy images for which image quality did not permit quantitative cone spacing measures were excluded from the analysis. Therefore, eight ROIs located over drusen from these three study eyes were not included in the longitudinal analysis. In addition, AOSLO images of ROIs GA1, GA2, and GA3 from patient 3 were not obtained at the 12-month visit, resulting in 9-months follow-up available for analysis of these regions. All other ROIs were followed longitudinally over 12 to 21 months.

Retinal Areas With No Geographic Atrophy or Drusen

Adaptive optics scanning laser ophthalmoscopy images from all 13 ROIs selected at retinal areas in which there was no evidence of drusen or GA revealed continuous photoreceptor mosaics. Within these mosaics, cones were noted as bright round or oval uniformly sized profiles that were arranged in an ordered array (Fig. 2). These features are consistent with previous reports of cone structure seen in AOSLO images from healthy eyes.[34,49]

At baseline, cone spacing measures were normal for all study eyes in regions showing no drusen or GA (Z scores = –0.6 to 1.54) (Fig. 3). Over the study period, all these retinal regions remained structurally unchanged and there was no evidence of formation of drusen or pigmentary abnormalities noted in clinical images or SD-OCT scans. There were variations in cone spacing measures between visits for some of these ROIs. However, cone spacing remained within the normal age-matched range in all of the 13 normal retinal regions followed over 12 to 21 months (Fig. 3). We interpret this to mean that no significant change in cone spacing occurred in healthy retinal regions in the study eyes during this period.

Retinal Areas Over Drusen

In all ROIs selected over drusen, AOSLO images showed unambiguous cone mosaics characterized by ordered packing. However, mild morphologic alterations were noted within these mosaics, including subtle irregularity and areas of reduced cone reflectivity. These often resulted in formation of a patchy, hyporeflective AOSLO signal in areas located over drusen (Fig. 4). The dark signal colocalized with hyporeflectivity of the IS/OS junction directly overlying drusen noted in registered SD-OCT images (Fig. 4).

At baseline, cone spacing measures were normal in all ROIs located over drusen (Z-scores = –1.88 to 2) except for two regions from one study eye (patient 6, right eye, locations D3 and D5). In this eye with extensive multiple drusenoid RPE detachments, we analyzed five drusen ROIs, of which cone spacing at baseline was marginally increased above the normal range in two (Z-scores = 2.71 and 2.98). Baseline SD-OCT images from both these regions showed hyporeflectivity of the IS/OS photoreceptor junction directly overlying each region with focal disruption near region D3 (Fig. 5).

During the study period, qualitative changes in drusen morphology were noted in SD-OCT images of several ROIs from a few study eyes. Progression of drusen was found in four regions of the 20 drusen ROIs for which follow-up AOSLO images were available for longitudinal analysis, and regression was noted in one other region. Furthermore, focal discontinuity or hyporeflectivity of the outer retinal band corresponding with the IS/OS layer overlying drusen was noted during the study period in 10 drusen regions. Nonetheless, there was no direct correlation between change in drusen morphology in clinical or SD-OCT images and changes noted in corresponding AOSLO images. No corresponding morphologic alterations were apparent in AOSLO images from any of the drusen

Investigative Ophthalmology & Visual Science

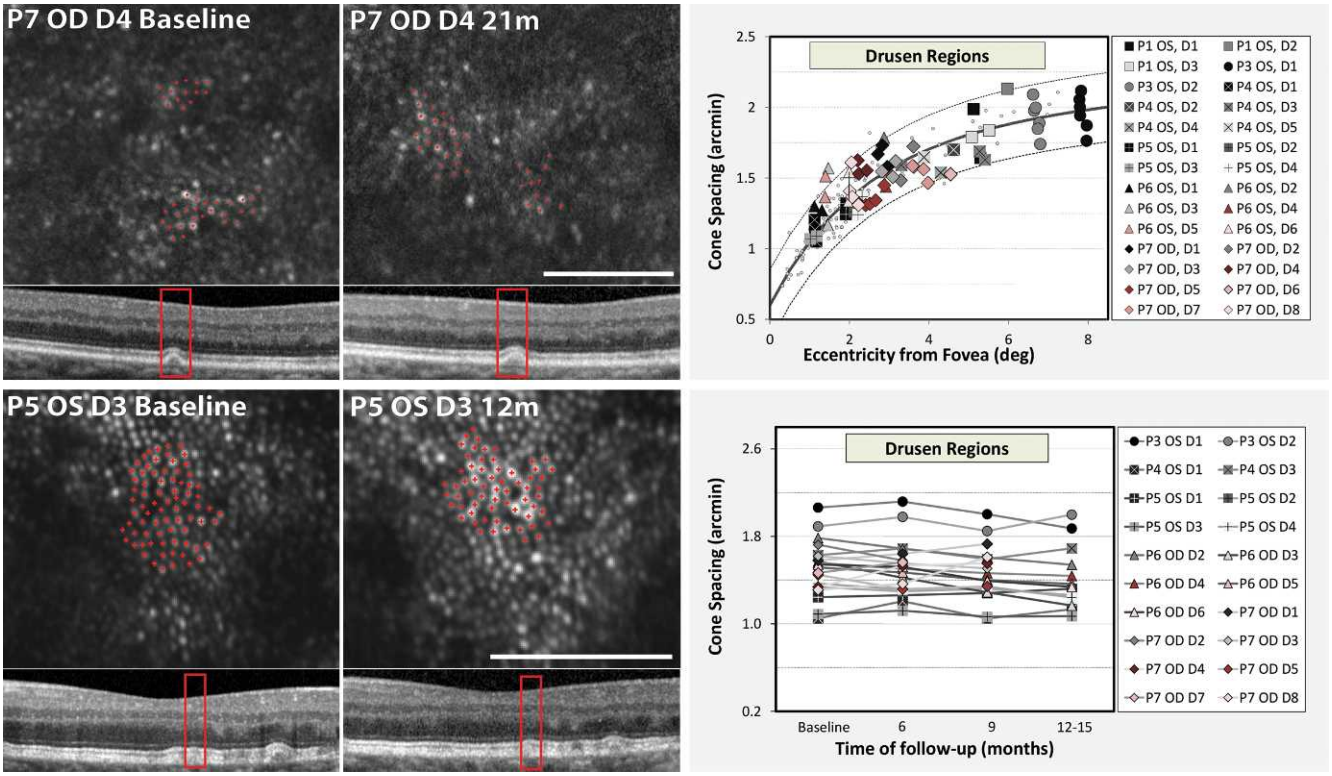

Figure 6. Cone spacing measurements in eyes with nonneovascular AMD at regions over drusen. *Left images*: AOSLO images and corresponding SD-OCT scans obtained from ROIs over drusen at baseline and at the last follow-up visit. Individual cones within mosaics identified in each AOSLO image are labeled by red cross-hairs. *Red bars* on OCT images denote the area for which a magnified AOSLO image is shown above. *Upper panel*: patient 7, right eye, location drusen 4. Spectral domain optical coherence tomography images show increased lateral extent and height of the druse at 21 months versus baseline. Cone spacing values obtained from this region were normal at baseline and remained within the normal range during the study. *Lower panel*: patient 5, left eye, location drusen 3. Registered SD-OCT images show stable drusen morphology in this ROI during the study period. Cone spacing values from this region were normal throughout the study period. *Upper right*: cone spacing measures from eyes with nonneovascular AMD and age-similar, visually healthy control subjects versus retinal eccentricity. Data from control subjects are plotted as *small gray dots. Dark solid line* indicates best fit to normal data. *Dashed lines*: 95% confidence limits of the best fit. Each ROI was imaged at several time points and multiple data-points are shown for each ROI to represent the serial spacing measures obtained during the study. *Lower right*: change in cone spacing measured at baseline and at each study visit for each ROI. All spacing values from all drusen ROIs remained within the normal range during the study period.

regions that exhibited changes in drusen height during the study period. Although mild variations were noted between different imaging sessions, AOSLO-derived cone spacing measures remained within the 95% CIs of the age-similar mean during the study period in all ROIs located over drusen, regardless of structural changes documented by multimodal imaging in these regions during the study (Fig. 6, right panels).

Junctional Areas Between Geographic Atrophy and Nonatrophic Retina

In all study eyes in which retinal regions adjacent to GA margins were analyzed, AOSLO imaging revealed continuous cone mosaics up to the edge of the atrophy, whereas no cone mosaics were unambiguously seen within the area of atrophy. As was also observed over drusen, AOSLO images from regions around GA margins revealed a transition zone in which the cone mosaics appeared qualitatively irregular with reduced cone reflectivity that often resulted in formation of a dark signal (Fig. 7, asterisks). The ring-shaped hyporeflective AOSLO signal colocalized with hyporeflectivity of the IS/OS junction layer noted in registered SD-OCT scans (Fig. 7). The hyporeflective AOSLO signal surrounding GA was noted in all follow-up AOSLO images from these regions. We found no correlation between the AOSLO dark signal and presence of adjacent hyperfluorescence in FAF images obtained throughout the study period (Supplementary Fig. S1).

At baseline, cone spacing measures were normal in all ROIs located at GA margins (Z scores = −1.93 to 1.3) except two ROIs from one study eye (patient 3, left eye, regions GA4 and GA5), in which cone spacing was marginally increased above normal (Z scores = 2.19 and 2.79). Both these ROIs were located near the edge of a small extrafoveal GA area (Figs. 1, 8). Baseline SD-OCT through both regions showed a continuous IS/OS photoreceptor junction layer. During the 15 months of study follow up, mild enlargement of the GA was noted in clinical images from this study eye, with extension of its margin towards the location of these two ROIs (Fig. 8). Nonetheless, cone spacing measures over time did not fall outside the normal distribution in both these regions. Similarly, although standard clinical measures showed progression of GA adjacent to some of the ROIs during the study period (Fig. 8), AOSLO longitudinal tracking demonstrated cone spacing measures that did not fall outside the normal age-matched range in all ROIs located at GA margins where cones were visualized, irrespective of clinical evidence of progression of the atrophy in that region (Fig. 8).

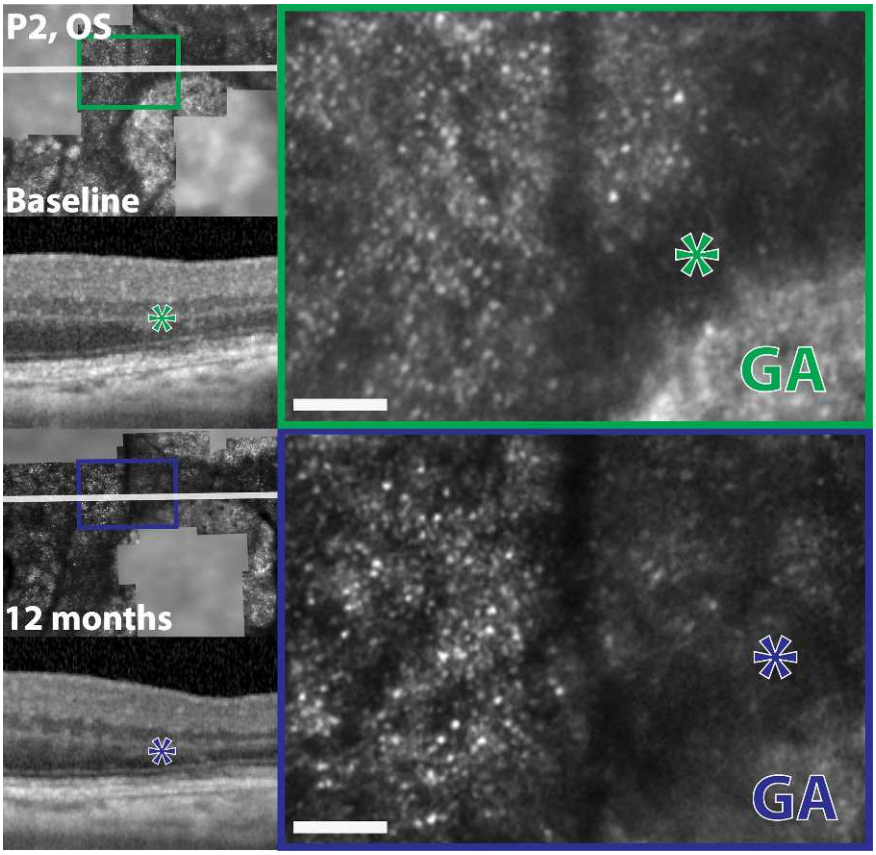

FIGURE 7. Morphologic features of AOSLO images in retinal areas adjacent to geographic atrophy margins. *Left column*: AOSLO images from ROI GA2 from the left eye of patient 2 at baseline and after 12 months of follow up are registered with infrared fundus images and SD-OCT scans. *White lines* indicate the location of the OCT sections, which skim the edges of the GA regions. The *green* and *dark blue boxes* (*left*) indicate areas of magnified AOSLO images shown in *green* and *dark blue insets* in the *right column*, respectively. Areas of reduced cone reflectivity seen as hyporeflective AOSLO signal around the margin of geographic atrophy correspond with hyporeflectivity of the IS/OS layer in the SD-OCT images (*asterisks*). *Scale bar*: 15 arc minutes.

DISCUSSION

Examination by high-resolution AOSLO images enables in vivo visualization of cone photoreceptors and allows quantitative measurement of cone spacing over drusen and at the margin of GA in eyes with AMD. We observed continuous cone mosaics with normal or near-normal cone spacing at most ROIs over drusen and at the margins of GA. Cone spacing measures in these regions as well as in retinal areas with no drusen or GA were within the same range of spacing values obtained in control eyes from age-similar subjects. In all study eyes, cone spacing in retinal regions over drusen or at GA margins that were followed longitudinally over 12 to 21 months remained similar to baseline values during the study period. Examination by clinical measures and SD-OCT showed morphologic changes in several study regions located over drusen and progression of GA in all study eyes during the study period. Nonetheless, correlated measures of cone spacing remained within the normal range in most study regions located over drusen and at GA margins, even when progression of the GA edge was noted to extend towards the ROI. Previous histologic studies of photoreceptor topography in aging eyes[14,17,18,50,51] showed retention of cones in the fovea with a tightly packed polygonal mosaic that looked similar to control eyes. In the parafoveal region a preferential loss of rods was noted, whereas cone IS appeared large and adjacent to each other even when no intervening rods were seen.[14,17,18] Thus, remodeling of surviving rods can potentially account for apparent preservation of cone mosaics and maintain normal spacing between them, as found in our study. Cone spacing is a robust, but conservative, measure of the structural integrity of the photoreceptor mosaic in eyes with AMD, and may not be a sensitive indicator of disease progression. Nonetheless, our finding of cone spacing measures that were within the normal age-matched range in regions where cones were unambiguously visualized suggests that diffuse cone loss may not be occurring in eyes with nonneovascular AMD. Further, persistence of cone spacing measures within the normal age-matched range over time may provide insight into the pathophysiology of progression of drusen and GA, suggesting that increased cone spacing may not be measurable in advance of local progression of AMD, and that cone spacing is preserved until disease progression is advanced.

Although we saw no quantifiable differences in cone spacing between AMD patients and healthy eyes, we did observe qualitative differences in the cone appearance in the images. The next two paragraphs summarize our subjective assessments of variations in cone reflectance and variations in cone packing geometry.

We found morphologic abnormalities of cone photoreceptor mosaics including irregular appearance and reduced cone reflectivity over drusen and around GA edges resulting in a hyporeflective AOSLO signal. These morphologic abnormalities were seen even in regions in which quantitative measures of cone spacing were normal, signifying possible disruption of the structural integrity of the photoreceptors in the absence of

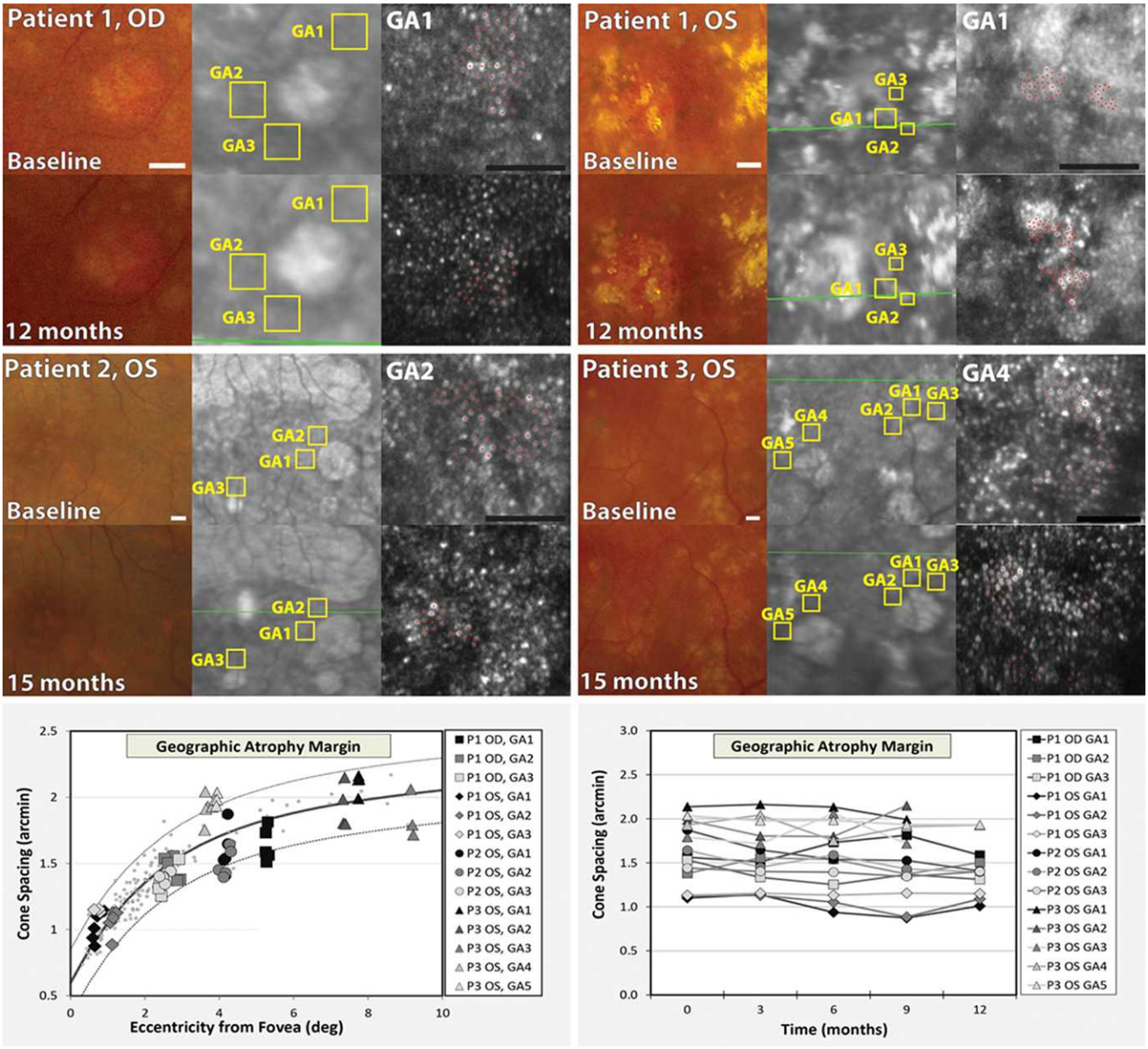

Figure 8. Cone spacing measurements in eyes with nonneovascular AMD near margins of geographic atrophy. For each study eye, images obtained from regions of interest at the margins of geographic atrophy at baseline and at the last follow-up visit, including color fundus photograph and infrared fundus image, are shown. Locations of ROIs identified at the margins of GA are denoted on each infrared image. A magnified AOSLO image from one ROI is shown on the *right* of each panel. On each magnified AOSLO image, individual cones identified are denoted with *red cross-hairs*. *White scale bar* on color fundus photographs: 200 μm. *Black scale bar* on AOSLO images: 15 arc minutes. *Upper left panel*: patient 1, right eye. *Upper right panel*: patient 1, left eye. *Lower right panel*: patient 2, left eye. *Lower right panel*: patient 3, left eye. *Lower left*: Cone spacing measures from eyes with nonneovascular AMD and age-similar visually healthy control subjects versus retinal eccentricity. Data from the control subjects are plotted as *small gray dots*. *Dark solid line* indicates best fit to normal data. *Dashed lines*: 95% confidence limits of the best fit. Patient 3 shows mildly increased cone spacing to the near-normal level at locations GA4 and GA5, but all other GA regions derived normal or near-normal cone spacing measures throughout the entire study period. *Lower right*: Cone spacing measures from all ROIs identified at GA margin versus follow-up time.

measurable increases in cone spacing. Comparison with registered OCT scans confirmed the presence of the photoreceptor IS/OS junction in the studied regions over drusen and at GA margins, although often characterized by hyporeflectivity. In contrast, AOSLO images from regions in which there was no evidence of drusen or GA on multimodal imaging showed continuous cone mosaics characterized by uniform reflectivity properties, similar to previously reported AOSLO observations in healthy eyes.[49,52] The hyporeflectivity of cones noted in AOSLO images over drusen or at GA margins could result from an optical misalignment of the photoreceptors caused by topographic irregularities such as the dome-shaped drusen elevation or excavation at the edge of GA, thus, disrupting their original orderly vertical arrangement and altering their wave-guiding characteristics.[47] Intraretinal pigment clumps lying above the photoreceptors may also give rise to apparent variance in their reflectivity,[53] although such findings were not seen in our study regions. Alternatively, our observations of regional compromise of photoreceptor structure in eyes with AMD could reflect photoreceptor stress occurring focally over

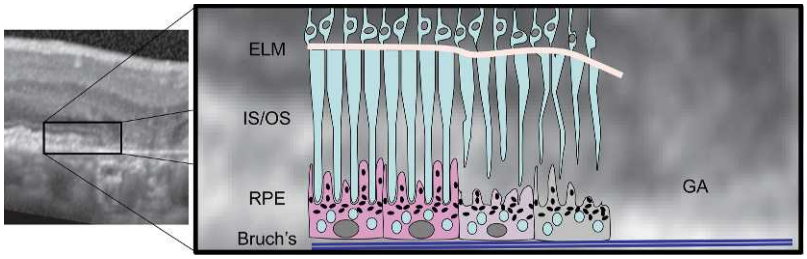

Figure 9. Proposed simplified model to explain loss of visibility of cones at the edge of advancing GA. Cones and RPE cells in regions without GA (left side of illustration and registered SD-OCT image) are closely packed, have near normal spacing and are easily imaged owing to their inherent wave-guiding properties. Closer to the GA, the RPE cell health is compromised, resulting in subsequent loss of cone wave-guiding properties, even though the cones are still present. Finally, the RPE cells along with their corresponding cones die to form a region of GA. Cones at the edge of GA are still present, but because their wave-guiding properties are compromised they are less visible in OCT and AOSLO images. Rods are not shown in this simplified model but their loss is assumed to take place through a similar mechanism.

drusen and at GA margins from compressing effect, compromised metabolic exchange or activation of the immune system.[16,54,55] Curcio et al.[14,17] studied photoreceptor loss in nonneovascular AMD and noted the greatest rod photoreceptor loss at the parafovea, although no focal changes in photoreceptor structure were recorded directly over drusen. Other histologic studies found photoreceptor density to be decreased over drusen,[15,16] and another postmortem study found photoreceptor abnormalities at the edge of GA that included shortening and bulging of the IS and fragmentation of the OS.[6] Such morphologic changes in the cones can disrupt the properties that make them such excellent waveguides and result in degraded reflectance properties such as those seen in our study. Several authors have similarly reported morphologic alterations seen on SD-OCT over drusen[19,56] or at the junctional zone of GA[24,25,57] in eyes with AMD. Consistent with our findings, Godara and associates[40] reported normal cone spacing over drusen using AOSLO in a 15-year-old boy with dominant drusen, and in a 45-year-old woman with basal laminar drusen,[37] although cones over drusen were hyperreflective.[37,40]

An important aspect of our study is that we used a subjective approach to assess the overall regularity of cone structure within a given ROI. In some regions, we also observed irregularity of the cone mosaic in a given ROI. While this qualitative method has the disadvantage of not providing objective, quantitative measures of mosaic geometry, we believe it to be an appropriate approach given the various technical issues with using techniques such as Voronoi analysis. Cone packing geometry can be analyzed graphically using Voronoi diagrams,[58,59] but this analysis is vulnerable to technical factors that can greatly affect its measure even in healthy eyes, including image resolution and variations in brightness and contrast of the cone mosaic. Therefore, Voronoi analysis should be done only in images with adequate quality where all cones are resolved, and as such was not performed in the present study. Our measures of the structural integrity of the cone mosaics did not include quantitative analysis of packing regularity and their topographic arrangement. Nonetheless, the irregular appearance of cone mosaics observed qualitatively in some study eyes even in regions where cone spacing measures were not different from the age-similar normal range suggests that changes in the geometric arrangement of cone mosaics may present a biomarker of early disease in eyes with AMD, when cone spacing measures are still preserved.

We anticipate that advances in AO technology will enable quantitative measures of cone reflectance variations and packing geometry, and that their potential value as biomarkers of AMD will be ascertained. Improved image quality with higher resolution to discern cone and rod structure,[60] along with more extensive image averaging will improve the ability to distinguish between missing and dim photoreceptors and permit quantitative assessments of photoreceptor structure noninvasively in eyes with AMD.

Our finding of continuous cone mosaics up to the GA margin, characterized by normal spacing measures, but abnormal morphology suggests that photoreceptor loss was directly coupled with RPE cell loss within the GA area. However, reduced visibility of cones around the GA edge may signify disruption of their wave-guiding properties that could also be explained by loss of adjacent RPE cells (Fig. 9). Although no pattern of abnormal hyperfluorescence was noted in corresponding FAF images from our study regions where hyporeflective AOSLO signal was seen (Supplementary Fig. S1), it is possible that compromised RPE cell function in the junctional zone around GA is associated with compromised metabolic or mechanical support of the overlying cones that changes their reflectance and packing arrangement.

Although AOSLO imaging is useful in delineating structural features of cone mosaics, it does not provide information regarding their cellular function. Our findings do not indicate the functionality of the cones within the studied retinal regions or the integrity of interactions between the cones and adjacent RPE cells. High-resolution assessment of visual function at drusen and GA margins locations showing hyporeflective AOSLO signals would provide insight into the impact drusen and GA have on cone function. Thus, our findings do not isolate the initiating event in GA progression as either cone photoreceptor, RPE, or choriocapillaris loss, but they do emphasize the intimate relationship between cone loss and RPE loss in eyes with GA. Future studies could use AOSLO microperimetry[61] to deliver stimuli to individual cones and measure function in retinal regions in which cones are visualized in eyes with AMD, comparing regions with normal cone spacing that have no drusen with function in regions with normal cone spacing over drusen and at the margins of GA to assess the impact of AMD on cone function prior to cone loss.

Potential limitations to our study include variations in AOSLO image quality, which resulted in some images that were insufficient for visualization of cones and quantitative analysis during the study, requiring removal of several drusen ROIs from the longitudinal analysis. Among elderly patients with AMD, several factors may preclude high AOSLO image quality, including poor fixation and higher rates of tear film abnormalities and media opacities, such as cataract. Further, as we analyzed cone structure only in retinal images with adequate quality to allow quantitative cone spacing measures, our results represent a very conservative measure of retinal health. Nonetheless, all other ROIs identified over drusen and at the

margin of GA were successfully followed longitudinally in a prospective manner, even in areas near progression of GA. Our findings demonstrate that AOSLO can be used to assess cone structure in patients with AMD and provide evidence of their preservation as targets for future therapeutic strategies.

In summary, our results suggest that AOSLO can provide adequate resolution for quantitative measurement of cone structure at the margin of GA and over drusen in eyes with nonneovascular AMD. Cone spacing over drusen and at the edges of GA was not different than normal in 26/28 and 12/14 ROIs measured, respectively, suggesting changes in cone spacing may not represent a primary structural change in AMD progression. However, abnormal morphologic features and reflectivity changes of cone mosaics noted at these locations may provide insight into the pathophysiology of GA progression.

Acknowledgments

Supported by grants from Alan Laties Career Development Award, Foundation Fighting Blindness (SZS); National Institutes of Health Grants EY002162, EY014375, Novartis Institutes for Biomedical Research, Foundation Fighting Blindness, Research to Prevent Blindness, Beckman Initiative for Macular Research (JLD), Bright-Focus Foundation (formerly The American Health Assistance Foundation), The Bernard A. Newcomb Macular Degeneration Fund, That Man May See, Inc., Hope for Vision (All JLD); University of California at San Francisco Research Allocation Program Novel Clinical/Translational Methods Award (RS); The George and Rosalie Hearst Foundation (MM); and the Novartis Institutes for Biomedical Research (EY014375; AR).

Disclosure: **S. Zayit-Soudry**, None; **J.L. Duncan**, None; **R. Syed**, None; **M. Menghini**, None; **A.J. Roorda**, P

References

1. Klein R, Klein BE, Jensen SC, Meuer SM. The five-year incidence and progression of age-related maculopathy: the Beaver Dam Eye Study. *Ophthalmology*. 1997;104:7–21.
2. Klein R, Klein BE, Tomany SC, Meuer SM, Huang GH. Ten-year incidence and progression of age-related maculopathy: the Beaver Dam Eye Study. *Ophthalmology*. 2002;109:1767–1779.
3. Pascolini D, Mariotti SP, Pokharel GP, et al. 2002 global update of available data on visual impairment: a compilation of population-based prevalence studies. *Ophthalmic Epidemiol*. 2004;11:67–115.
4. Mitchell P, Smith W, Attebo K, Wang JJ. Prevalence of age-related maculopathy in Australia. The Blue Mountains Eye Study. *Ophthalmology*. 1995;102:1450–1460.
5. Gass JD. Drusen and disciform macular detachment and degeneration. *Arch Ophthalmol*. 1973;90:206–217.
6. Sarks JP, Sarks SH, Killingsworth MC. Evolution of geographic atrophy of the retinal pigment epithelium. *Eye (Lond)*. 1988; 2(Pt 5);552–577.
7. Dunaief JL, Dentchev T, Ying GS, Milam AH. The role of apoptosis in age-related macular degeneration. *Arch Ophthalmol*. 2002;120:1435–1442.
8. Hageman GS, Luthert PJ, Victor Chong NH, Johnson LV, Anderson DH, Mullins RF. An integrated hypothesis that considers drusen as biomarkers of immune-mediated processes at the RPE-Bruch's membrane interface in aging and age-related macular degeneration. *Prog Retin Eye Res*. 2001;20: 705–732.
9. Lutty G, Grunwald J, Majji AB, Uyama M, Yoneya S. Changes in choriocapillaris and retinal pigment epithelium in age-related macular degeneration. *Mol Vis*. 1999;5:35.
10. Holz FG, Pauleikhoff D, Klein R, Bird AC. Pathogenesis of lesions in late age-related macular disease. *Am J Ophthalmol*. 2004;137:504–510.
11. Weiter JJ, Delori FC, Wing GL, Fitch KA. Retinal pigment epithelial lipofuscin and melanin and choroidal melanin in human eyes. *Invest Ophthalmol Vis Sci*. 1986;27:145–152.
12. Wing GL, Blanchard GC, Weiter JJ. The topography and age relationship of lipofuscin concentration in the retinal pigment epithelium. *Invest Ophthalmol Vis Sci*. 1978;17:601–607.
13. Holz FG, Bellman C, Staudt S, Schutt F, Volcker HE. Fundus autofluorescence and development of geographic atrophy in age-related macular degeneration. *Invest Ophthalmol Vis Sci*. 2001;42:1051–1056.
14. Curcio CA, Medeiros NE, Millican CL. Photoreceptor loss in age-related macular degeneration. *Invest Ophthalmol Vis Sci*. 1996;37:1236–1249.
15. Johnson PT, Brown MN, Pulliam BC, Anderson DH, Johnson LV. Synaptic pathology, altered gene expression, and degeneration in photoreceptors impacted by drusen. *Invest Ophthalmol Vis Sci*. 2005;46:4788–4795.
16. Johnson PT, Lewis GP, Talaga KC, et al. Drusen-associated degeneration in the retina. *Invest Ophthalmol Vis Sci*. 2003; 44:4481–4488.
17. Curcio CA. Photoreceptor topography in ageing and age-related maculopathy. *Eye (Lond)*. 2001;15:376–383.
18. Jackson GR, Owsley C, Curcio CA. Photoreceptor degeneration and dysfunction in aging and age-related maculopathy. *Ageing Res Rev*. 2002;1:381–396.
19. Schuman SG, Koreishi AF, Farsiu S, Jung SH, Izatt JA, Toth CA. Photoreceptor layer thinning over drusen in eyes with age-related macular degeneration imaged in vivo with spectral-domain optical coherence tomography. *Ophthalmology*. 2009; 116:488–496, e482.
20. Klein ML, Ferris FL III, Armstrong J, et al. Retinal precursors and the development of geographic atrophy in age-related macular degeneration. *Ophthalmology*. 2008;115:1026–1031.
21. Sunness JS, Margalit E, Srikumaran D, et al. The long-term natural history of geographic atrophy from age-related macular degeneration: enlargement of atrophy and implications for interventional clinical trials. *Ophthalmology*. 2007;114:271–277.
22. Holz FG, Bindewald-Wittich A, Fleckenstein M, Dreyhaupt J, Scholl HP, Schmitz-Valckenberg S. Progression of geographic atrophy and impact of fundus autofluorescence patterns in age-related macular degeneration. *Am J Ophthalmol*. 2007; 143:463–472.
23. Schmitz-Valckenberg S, Bindewald-Wittich A, Dolar-Szczasny J, et al. Correlation between the area of increased autofluorescence surrounding geographic atrophy and disease progression in patients with AMD. *Invest Ophthalmol Vis Sci*. 2006; 47:2648–2654.
24. Bearelly S, Chau FY, Koreishi A, Stinnett SS, Izatt JA, Toth CA. Spectral domain optical coherence tomography imaging of geographic atrophy margins. *Ophthalmology*. 2009;116:1762–1769.
25. Fleckenstein M, Charbel Issa P, Helb HM, et al. High-resolution spectral domain-OCT imaging in geographic atrophy associated with age-related macular degeneration. *Invest Ophthalmol Vis Sci*. 2008;49:4137–4144.
26. Fleckenstein M, Schmitz-Valckenberg S, Adrion C, et al. Tracking progression with spectral-domain optical coherence tomography in geographic atrophy caused by age-related macular degeneration. *Invest Ophthalmol Vis Sci*. 2010;51: 3846–3852.
27. Yehoshua Z, Rosenfeld PJ, Gregori G, et al. Progression of geographic atrophy in age-related macular degeneration imaged with spectral domain optical coherence tomography. *Ophthalmology*. 2011;118:679–686.
28. Choi SS, Doble N, Hardy JL, et al. In vivo imaging of the photoreceptor mosaic in retinal dystrophies and correlations with visual function. *Invest Ophthalmol Vis Sci*. 2006;47: 2080–2092.

29. Liang J, Williams DR, Miller DT. Supernormal vision and high-resolution retinal imaging through adaptive optics. *J Opt Soc Am A Opt Image Sci Vis*. 1997;14:2884–2892.
30. Roorda A, Romero-Borja F, Donnelly III WJ, Queener H, Hebert T, Campbell M. Adaptive optics scanning laser ophthalmoscopy. *Opt Express*. 2002;10:405–412.
31. Zhang Y, Poonja S, Roorda A. MEMS-based adaptive optics scanning laser ophthalmoscopy. *Opt Lett*. 2006;31:1268–1270.
32. Carroll J. Adaptive optics retinal imaging: applications for studying retinal degeneration. *Arch Ophthalmol*. 2008;126:857–858.
33. Chen Y, Ratnam K, Sundquist SM, et al. Cone photoreceptor abnormalities correlate with vision loss in patients with Stargardt disease. *Invest Ophthalmol Vis Sci*. 2011;52:3281–3292.
34. Duncan JL, Zhang Y, Gandhi J, et al. High-resolution imaging with adaptive optics in patients with inherited retinal degeneration. *Invest Ophthalmol Vis Sci*. 2007;48:3283–3291.
35. Talcott KE, Ratnam K, Sundquist SM, et al. Longitudinal study of cone photoreceptors during retinal degeneration and in response to ciliary neurotrophic factor treatment. *Invest Ophthalmol Vis Sci*. 2011;52:2219–2226.
36. Wolfing JI, Chung M, Carroll J, Roorda A, Williams DR. High-resolution retinal imaging of cone-rod dystrophy. *Ophthalmology*. 2006;113:1019, e1011.
37. Godara P, Siebe C, Rha J, Michaelides M, Carroll J. Assessing the photoreceptor mosaic over drusen using adaptive optics and SD-OCT. *Ophthalmic Surg Lasers Imaging*. 2010;41(suppl):S104–S108.
38. Roorda A, Zhang Y, Duncan JL. High-resolution in vivo imaging of the RPE mosaic in eyes with retinal disease. *Invest Ophthalmol Vis Sci*. 2007;48:2297–2303.
39. Morgan JI, Dubra A, Wolfe R, Merigan WH, Williams DR. In vivo autofluorescence imaging of the human and macaque retinal pigment epithelial cell mosaic. *Invest Ophthalmol Vis Sci*. 2009;50:1350–1359.
40. Godara P, Wagner-Schuman M, Rha J, Connor TB, Stepien KE, Carroll J. Imaging the photoreceptor mosaic with adaptive optics: beyond counting cones. In: LaVail M, Ash J, Anderson R, Hollyfield J, Grimm C, eds. *Retinal Degenerative Diseases*. New York: Springer; 2012:451–458.
41. Boretsky A, Khan F, Burnett G, et al. In vivo imaging of photoreceptor disruption associated with age-related macular degeneration: a pilot study. *Lasers Surg Med*. 2012;44:603–610.
42. Spaide RF, Curcio CA. Anatomical correlates to the bands seen in the outer retina by optical coherence tomography: literature review and model. *Retina*. 2011;31:1609–1619.
43. Hartmann KI, Gomez ML, Bartsch DU, Schuster AK, Freeman WR. Effect of change in drusen evolution on photoreceptor inner segment/outer segment junction. *Retina*. 2012;32:1492–1499.
44. Stevenson SB, Roorda A. Correcting for miniature eye movements in high resolution scanning laser ophthalmoscopy. In: Manns Fabrice PGS, Ho, Arthur, Stuck, Bruce E, Belkin Michael, ed. *Ophthalmic Technologies XV*. Bellingham, WA: SPIE; 2005;145–151.
45. Vogel CR, Arathorn DW, Roorda A, Parker A. Retinal motion estimation in adaptive optics scanning laser ophthalmoscopy. *Opt Express*. 2006;14:487–497.
46. Roorda A, Metha AB, Lennie P, Williams DR. Packing arrangement of the three cone classes in primate retina. *Vision Res*. 2001;41:1291–1306.
47. Roorda A, Williams DR. Optical fiber properties of individual human cones. *J Vis*. 2002;2:404–412.
48. Ferris FL III, Wilkinson CP, Bird A, et al. Clinical classification of age-related macular degeneration. *Ophthalmology*. 2013;120:844–851.
49. Chui TY, Song H, Burns SA. Adaptive-optics imaging of human cone photoreceptor distribution. *J Opt Soc Am A Opt Image Sci Vis*. 2008;25:3021–3029.
50. Curcio CA, Millican CL, Allen KA, Kalina RE. Aging of the human photoreceptor mosaic: evidence for selective vulnerability of rods in central retina. *Invest Ophthalmol Vis Sci*. 1993;34:3278–3296.
51. Panda-Jonas S, Jonas JB, Jakobczyk-Zmija M. Retinal photoreceptor density decreases with age. *Ophthalmology*. 1995;102:1853–1859.
52. Merino D, Duncan JL, Tiruveedhula P, Roorda A. Observation of cone and rod photoreceptors in normal subjects and patients using a new generation adaptive optics scanning laser ophthalmoscope. *Biomed Opt Express*. 2011;2:2189–2201.
53. Gocho K, Sarda V, Falah S, et al. Adaptive optics imaging of geographic atrophy. *Invest Ophthalmol Vis Sci*. 2013;54:3673–3680.
54. Gu J, Pauer GJ, Yue X, et al. Assessing susceptibility to age-related macular degeneration with proteomic and genomic biomarkers. *Mol Cell Proteomics*. 2009;8:1338–1349.
55. Yu Y, Reynolds R, Rosner B, Daly MJ, Seddon JM. Prospective assessment of genetic effects on progression to different stages of age-related macular degeneration using multistate Markov models. *Invest Ophthalmol Vis Sci*. 2012;53:1548–1556.
56. Yi K, Mujat M, Park BH, et al. Spectral domain optical coherence tomography for quantitative evaluation of drusen and associated structural changes in non-neovascular age-related macular degeneration. *Br J Ophthalmol*. 2009;93:176–181.
57. Brar M, Kozak I, Cheng L, et al. Correlation between spectral-domain optical coherence tomography and fundus autofluorescence at the margins of geographic atrophy. *Am J Ophthalmol*. 2009;148:439–444.
58. de Monasterio FM, McCrane EP, Newlander JK, Schein SJ. Density profile of blue-sensitive cones along the horizontal meridian of macaque retina. *Invest Ophthalmol Vis Sci*. 1985;26:289–302.
59. Li KY, Roorda A. Automated identification of cone photoreceptors in adaptive optics retinal images. *J Opt Soc Am A Opt Image Sci Vis*. 2007;24:1358–1363.
60. Dubra A, Sulai Y, Norris JL, et al. Noninvasive imaging of the human rod photoreceptor mosaic using a confocal adaptive optics scanning ophthalmoscope. *Biomed Opt Express*. 2011;2:1864–1876.
61. Tuten WS, Tiruveedhula P, Roorda A. Adaptive optics scanning laser ophthalmoscope-based microperimetry. *Optom Vis Sci*. 2012;89:563–574.

Investigative Ophthalmology & Visual Science